Appl. Phys. A 79, 647–659 (2004)
DOI: 10.1007/s00339-002-2075-3

Applied Physics A
Materials Science & Processing

K.G. DASSIOS
C. GALIOTIS✉

Fluorescence studies of polycrystalline Al_2O_3 composite constituents: piezo-spectroscopic calibration and applications

Institute for Chemical Engineering and High Temperature Processes, Foundation of Research & Technology-Hellas (FORTH), PO Box 1414, 26500 Patras, Greece

Received: 7 June 2002/Accepted: 23 November 2002
Published online: 28 March 2003 •

ABSTRACT Optical fluorescence microscopy (OFM) was used to quantify the effect of applied stress or strain upon the position of the R fluorescence line of α-Al_2O_3 composite constituents (fibers and matrices) prior to composite processing. Polycrystalline Nextel^{TM} Nextel 720 fibers were tested under tension and compression by means of a cantilever beam technique, whereas the polycrystalline matrix was tested in compression. The position of the R fluorescence line was correlated to applied strain and stress in order to provide the piezo-spectroscopic calibration curve and the corresponding coefficients for both sensors, which form the basis for interpretation of frequency shifts from full, all-alumina, composites. The piezo-spectroscopic coefficients of the polycrystalline matrix were found to be 2.57 cm^{-1} GPa^{-1} and 2.52 cm^{-1} GPa^{-1} for the R1 and R2 lines respectively, whereas the coefficients for the polycrystalline α-Al_2O_3 Nextel 720 fibers were found to be 3.07 cm^{-1} GPa^{-1} and 2.91 cm^{-1} GPa^{-1} for the R1 and R2 lines, respectively. The effects of collection probe size, as well as penetration depth, are discussed. The established piezo-spectroscopic behavior is used inversely to quantify the residual stresses in the as-received fibers due to the presence of sizing, as well as in the thermally grown alumina layer of an industrial thermal barrier coating.

PACS 87.64.Ni; 81.05.Je; 78.66.Sq

1 Introduction

Owing to their inherent oxidation-saturated characteristic, composite materials of metal oxide constituents have the ability to maintain their chemical stability and mechanical properties at high temperatures under severe oxidative and corrosive conditions. Over the last two decades, these advantageously featured materials have been effectively replacing metallic parts in high-temperature applications where the demand for durability, toughness and strength is of crucial importance for the structural integrity of components, such as combustion chamber liners, diffusor rings and other thermal protection systems for high-temperature applications in oxidizing environments. One of the most important metal oxide ceramics is aluminum oxide (alumina, Al_2O_3) which combines extreme hardness, wear and abrasion resistance, chemical inertness, outstanding electrical and electronic properties, good thermal shock resistance, dimensional stability and high mechanical strength at elevated temperatures [1]. As such, alumina has been implemented in advanced ceramic composite systems in various forms of constituents (fibers, whiskers, platelets, matrices, thermal barrier coatings etc.) with significant contribution to overcoming the problems of chemical sensitivity and limited working time at high temperatures that are associated with conventional ceramic constituents like C and SiC.

The use of alumina composite structures has increased along with pertinent research efforts to assess the mechanical behavior of such composites in order to improve performance, as well as manufacturing and processing routes. The macromechanical quantification of the properties of alumina composites and their fracture behavior provides only semi-quantitative estimates of the overall performance as it does not take into account the effects of active micromechanical aspects such as the variations within the reinforcing phase and the interactions between the composite phases, which can significantly influence the mechanical behavior of the system. On the other hand, such microscale characteristics can be directly quantified using diffraction and spectroscopic techniques. Raman spectroscopy and fluorescence spectroscopy are the most precise and versatile of these techniques since, contrary to X-ray and neutron diffraction techniques, they allow for high spatial resolutions and large penetration depths. Given the intense luminescence properties of alumina, the technique of optical fluorescence microscopy (OFM) has been established as the most powerful experimental method for assessing the micromechanics of deformation in single- and multi-phase alumina systems [2–21].

The principle of OFM is the quantification of frequency changes (shifts) of the fluorescence spectrum of a photoluminescent material with respect to strain or stress; a phenomenon known as the piezo-spectroscopic effect. The relatively fine hexagonal crystal structure of α-Al_2O_3 contains traces of Cr^{3+} ions substituting for the smaller Al^{3+} ions. Upon photostimulation, the excited Cr^{3+} relax back to the ground state by emitting radiation at characteristic frequencies, such as the prominent R fluorescence line shown in Fig. 1. The inherent asymmetry of the crystal along one axis of the lattice caused by the substitution of Al^{3+} ions by Cr^{3+} ions results in the

✉ Fax: +30-610/965-223, E-mail: c.galiotis@iceht.forth.gr

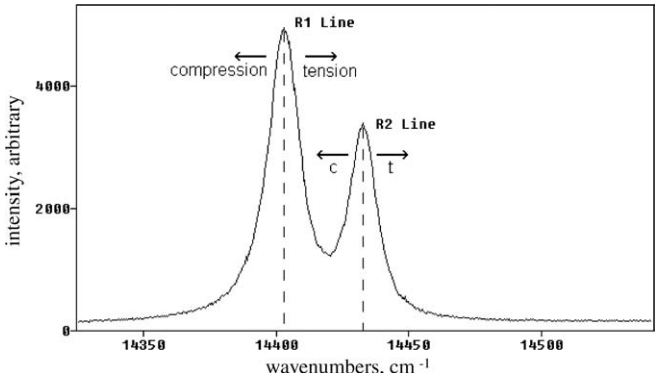

FIGURE 1 The prominent R fluorescence line of alumina consisting of the doublet R1 and R2 lines. Compressive loads shift the lines to lower frequencies whereas tensile loads have the opposite effect

splitting of the R fluorescence band into the R1 and R2 lines that appear at wave numbers of 14 403 and 14 433 cm^{-1}, respectively. The application of stress distorts the interatomic distances in the crystal field, changes the potential energy of the chromium ion and, as a result, alters the corresponding frequencies of these radiative transitions. In that sense, the wave number shifts of R fluorescence lines are indicative of the response of alumina to externally applied stress or strain. A tensile field causes the R fluorescence line to shift to higher wave numbers, whereas compressive loads have the opposite effect. Thus, the R fluorescence line can serve as a reliable deformation sensor for monitoring the micromechanical behavior of α-Al_2O_3 by calibrating its spectroscopic response to strain or stress (R line calibration curve).

The fluorescence spectrum of chromium-doped alumina has been effectively analyzed since the late 1950s and is today well established [2–4]. The first applied use of the piezo-spectroscopic effect of alumina appeared in 1978 [5] when the R line fluorescence was used as a residual stress sensor for a sintered monolithic alumina. However, it was not until the mid 1990s that more concerted interest was shown in quantifying the piezo-spectroscopic properties of the R line and in obtaining the corresponding piezo-spectroscopic coefficients that correlate the deformation level of an alumina to the exhibited shift of its R line [6–9]. During the last decade, a number of studies have focused on the measurement of stresses in both single-crystal and polycrystalline alumina systems using the shift of the R line fluorescence; a technique which essentially utilizes piezo-spectroscopic calibration in an inverse manner. The basic concept of these techniques is to use the R line calibration curve to interpret a measured shift by means of strain or stress. A wide overview of the fundamentals of this technique has previously appeared [10]. Known applications of the OFM technique include the measurement of residual stresses in transparent sapphire fibers embedded in γ-TiAl and Al_2O_3 matrices [11], the investigation of fiber strain change and interfacial failure during mechanical stressing in PRD-166/SLS glass matrix model composites [12], the determination of alumina Nextel 610 fiber strength from bundle tests by deconvolution of the R line to load-carrying and failed-fiber contributions [13] as well as the quantification of residual stresses developed during thermal oxidation of aluminum in thermal barrier coatings [14–17]. Additionally, the OFM technique has been used for the in situ determination of bridging stresses in Al_2O_3/Al_2O_3-platelet-reinforced composites [18], in Al_2O_3/molybdenum-particle-reinforced composites [19] as well as in large-grained alumina polycrystals [20]. A detailed study of the polarization dependence of the R line and its importance in the interpretation of the collected fluorescence spectra was conducted in 1997 [21] and the piezo-spectroscopic coefficients for chromium-doped alumina were revisited, along with findings of non-linear and rotational symmetry effects.

The extensive and successful application of the OFM technique in measuring stresses and strains in single-crystal or polycrystalline aluminas and in basic model composites has established it as a highly efficient and precise method for mechanical measurements at the microscale of such systems. On the other hand, the technique has not been applied in real composite systems such as fiber-reinforced ceramic matrix composites (CMCs) and other contemporary composites employing alumina constituents, which are currently considered state-of-the-art materials for many automotive, aerospace and defense applications. In particular, all-alumina composites comprising of high-strength Al_2O_3 fibers embedded in Al_2O_3 matrix find an increasing use in high-temperature structural/load-bearing applications. For such composites, one could determine independently the stress/strain distribution in the fibers and also in the matrix by means of OFM. In addition, important parameters that govern the mechanical performance of these composites, such as the residual stresses in both fiber and matrix, the stress transfer profiles and the fiber bridging stresses in the presence of matrix cracks, can be measured directly.

The primary step in the development of an all-alumina composite stress/strain sensor is the systematic study using OFM of the effect of applied stress or strain upon both fibers and matrix independently prior to composite processing. To this end, in situ OFM measurements have been conducted on both aluminosilicate fibers (3M Nextel^{TM} 720) and pure alumina matrices by calibrating their R1 and R2 fluorescence line shifts during tensile and compressive (for the matrix) tests. Furthermore, investigations have been performed on crucial aspects of OFM and their contribution to the application of this technique to specific alumina systems, and these are: (a) the significance of the dimensions of the collection probe relative to the grain size of the target alumina sensor; and (b) the determination of the penetration depth in α-Al_2O_3 and its significance in OFM measurements. The established piezo-spectroscopic behavior is used inversely to quantify the residual stresses due to thermal expansion mismatch in the alumina thermally grown oxide (TGO) of an industrial thermal-barrier coating material. Another application of the technique was the quantification of the residual stress field in the as-received fibers due to the presence of sizing.

2 Experimental set-up for fluorescence measurements

The ReRaM experimental set-up developed by Galiotis et al. [22] was used for the fluorescence measurements. A detailed description of the spectroscopic set-up along with the mechanical testing set-up is shown in Fig. 2. A detailed description of the fundamentals of the ReRaM

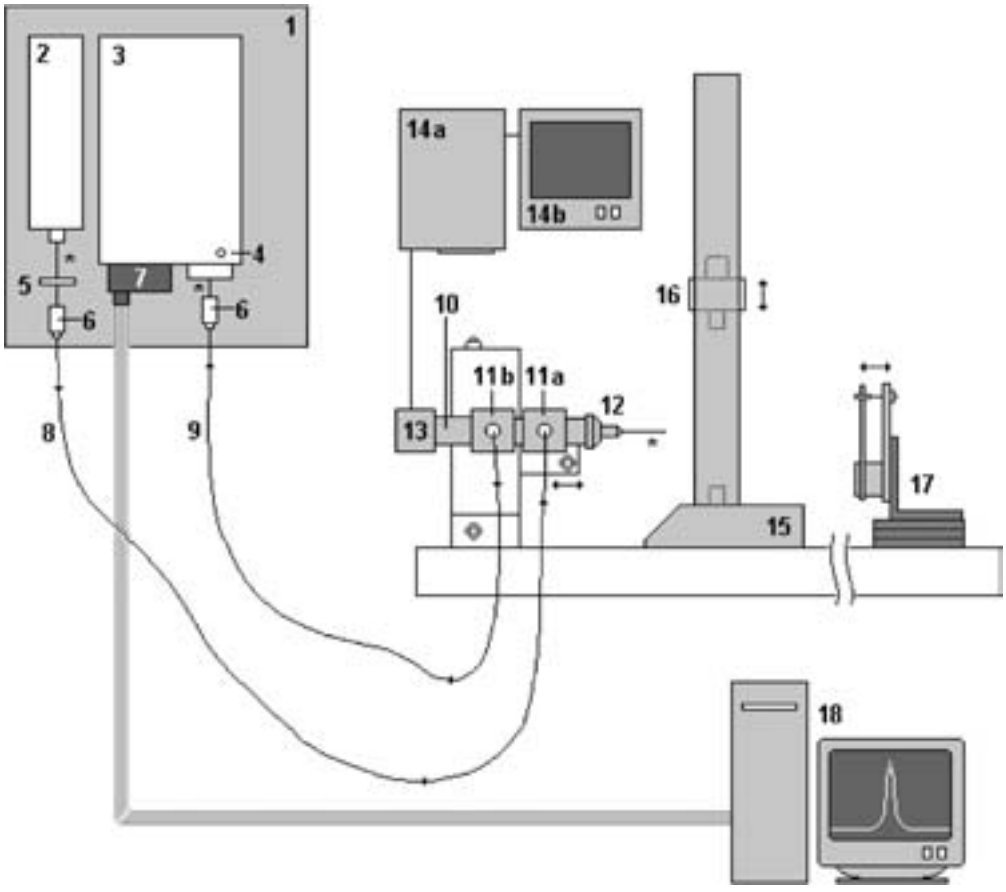

FIGURE 2 The ReRaM and mechanical testing system set-up

1. Vibration-free table
2. Lexel 95 argon-ion laser
3. SPEX 1000 M single monochromator
4. Slit control
5. Controllable attenuator
6. Fiber optic receptor assembly
7. CCD detector
8. Delivery fiber optic
9. Collection fiber optic
10. Olympus microscope
11. a. Delivery fiber optic receptor with beam splitter. b. Collection fiber optic receptor with notch filter
12. Objective lens
13. CCTV camera
14. Video copy processor (a) and monitor (b)
15. Mechanical testing frame with 20 kN load cell
16. Crosshead
17. Cantilever beam rig
18. PC with data acquisition software

* laser beam

set-up can be found in [23] and [24]. The fluorescence excitation source was produced by an argon-ion laser and had a wavelength of 514.5 nm. The monochromatic excitation radiation was polarized in the same direction to the loading axis; high-performance polarization-preserving fiber optics were used for delivery and collection of light. A Hounsfield type H20KM mechanical frame equipped with a 20 kN load cell was used for testing the matrix specimens in axial compression, whereas the fibers were tested in bending using a cantilever beam rig that produced a tensile or compressive stress gradient along the fiber length [25]. The laser microscope was attached to a 3-D translational stage with step-motion ability in each direction with a resolution of a few micrometers. The whole system was positioned in front of the mechanical testing machine or cantilever beam rig and was used to collect signals from the materials in real testing time. Different objective lenses were used to produce laser probe volumes of different sizes depending on the grain morphology of the materials investigated. This topic is discussed to extent in a following section. The mechanical testing machine, along with the spectroscopic set-up, rested on a vibration-free table.

An incident laser power of 1 mW, an integration time of 1 s (5 s for the case of fibers) and an inlet aperture (slit) of 50 μm on the SPEX 1000M single monochromator yielded very sharp fluorescence spectra. The exposure times were chosen as a result of the different penetration depths of the materials; the signal from the fibers was weaker as the laser probe penetrated to a smaller depth, and a higher exposure time was required to obtain spectra with good width/height ratios. The calibration of the system was achieved using the reference line of an argon-ion lamp at 14 357 cm^{-1} and the positions of the R1 and R2 peaks was verified with an independent spectroscopic system (Jobin Yvon T64000).

3 Methodology for the calibration of the piezo-spectroscopic effect

3.1 *Reference materials and specimens*

3.1.1 Fibers. The piezo-spectroscopic calibration of the fibers was performed on transparent alumina Nextel™ 720 (3M Corporation) mono-filaments extracted from a tow (specific lot number: A0177-0199). This fiber is established today as

Property	Value
Use temperature °C (application dependent)	1200
Filament diameter, μm	10 – 12
Crystal size, nm	< 500
Crystal structure	α-Al_2O_3+3Al_2O_3×2SiO_2 (mullite)
Density, g/cm^3	3.4
Chemical composition, (wt.%)	85 Al_2O_3, 15 SiO_2
Thermal expansion, ppm/°C (100–1100 °C)	6.0
Tensile strength, MPa (25 mm gauge length)	2100
Tensile modulus, GPa	260
Creep rate, 1/s (1100 °C/70 MPa)	$< 1 \times 10^{-10}$

TABLE 1 Typical Properties of Nextel^{TM} 720 fibers [26]

one of the most renowned ceramic types of reinforcement for continuous fiber-reinforced ceramic-matrix composites (CFCCs) and is claimed to combine excellent strength with high creep resistance. In the as-received form, Nextel^{TM} 720 fibers are coated with a polyvinyl alcohol sizing (the exact synthesis is not given by the company). The general properties of the fibers at room temperature, as reported by the manufacturer [26], are listed in Table 1. The crystal structure of the fiber – as verified through its fluorescence spectrum – is alpha-alumina (α-Al_2O_3).

Single-filament specimens to be tested in air using the cantilever beam bending technique (described in a following section) were prepared by extracting Nextel 720 fibers from the tow and subsequently bonding them along the length of a water-clear transparent PMMA beam (type Perspex^{TM}, ICI Acrylics Inc.). The beam material was chosen to satisfy the conditions of fluorescence inactivity in the R fluorescence region of alumina as well as mechanical durability to 1.5% strain. The fiber was bonded to the beam surface by lightly spraying it with a transparent acrylic coating (Levis acrylic satin varnish 90), which was also fluorescence-inactive in the spectral region of interest. The film, with a thickness of a few microns, was left to dry for 24 h. The fibers were subjected to a uniform stress along their cross section as the stress at the PMMA beam surface was directly transferred to the fiber via the adhesive material.

3.1.2 Matrix. The alumina matrix was produced by hot pressing of alumina powder at 1600 °C. This resulted in a tough non-porous polycrystalline material, the typical properties of which are presented in Table 2. The crystal structure of the matrix – as verified through its fluorescence spectrum – is also α-Al_2O_3. Matrix specimens to be tested in axial compression were machined in the form of 6 mm × 8 mm × 40 mm rectangular bars. These dimensions were evaluated under the Eulerian critical buckling load condition so that the specimen would not bend under compression.

Property	Value
Chemical composition, wt.%	> 99% Al_2O_3
Density, g/cm^3	3.97
Thermal expansion, ppm/°C (100–1100 °C)	8.0
Compressive strength, MPa	2945
Young's modulus, GPa	345–409

TABLE 2 Typical Properties of dense alumina [1]

3.2 *Experimental methodology*

3.2.1 Fibers–cantilever beam bending. Single as-received Nextel^{TM} 720 fibers were mounted on plastic beams and were tested in air using the cantilever beam technique [25], which ensures a uniform load across the fiber cross section combined with a stress gradient along the fiber length. A schematic representation of the cantilever beam rig can be found in Fig. 3. One end of the beam was fixed, whereas an adjustable screw (deflector) near the free end of the beam could flex the beam up or down to subject the top surface of the beam (and thus also the fiber) to compressive or tensile loads respectively. The deflection of the beam was measured by a dial gauge micrometer and was used to determine the strain distribution along the fiber length. On the beam, the maximum stress is found at the fixed end where the deflection is zero and the minimum stress is found at the free end, at the point of maximum deflection.

The strain distribution $\varepsilon(x)$ along the length of the beam (and thus also along the length of the fiber) at a distance x from the fixed end is given as a function of the geometry of the beam and the free-end deflection δ_{max} according to the equation [25]:

$$\varepsilon(x) = \frac{3t\delta_{max}}{2L^2}\left(1 - \frac{x}{L}\right) \quad (1)$$

where t is the beam thickness and L is the distance between the free and fixed ends. By measuring the maximum deflection at the free end, the strain gradient along the fiber can be obtained.

A 3-D micro-positioning stage with a step-motion ability of 1 μm in each direction was used to move the rig with respect to the laser probe, thus enabling the probe to scan the

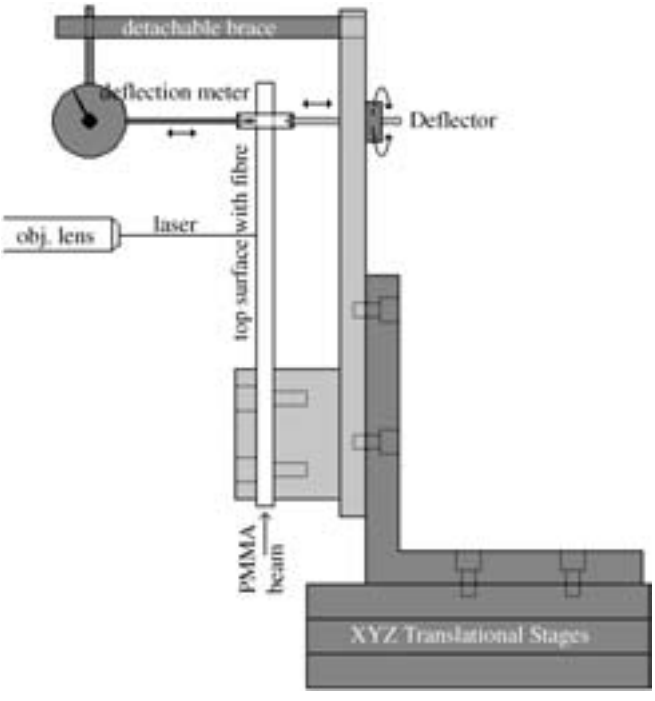

FIGURE 3 The cantilever-beam rig used for testing single fibers in air

fiber length with a fixed step. A high-magnification objective lens was used for collecting the spectra; a detailed discussion on the significance of probe volume is presented in Sect. 6. To establish the exact position of the reference R line of the stress-free state, five spectra were collected initially at random positions along the fiber. The beam was then flexed to produce a strain gradient along the beam surface with a maximum value (at the fixed end) of 1% and fluorescence spectra were collected along the fiber length at known distances from the fixed end. The spectra were subsequently analyzed to determine the wave-number shift of the R line from the stress-free value and correlated to the strain level corresponding to the specific collection point. Ultimately, the shift of the R line was plotted versus fiber strain to produce the piezo-spectroscopic calibration curve for the alumina fibers, as is presented in Sect. 4.

3.2.2 Matrix–axial compression. Alumina matrix specimens in the form of rectangular bars were tested in axial compression. Compressive load was applied with a rate of 500 N/min and double strain gages were attached symmetrically on opposite faces of the specimen for direct strain measurement (Fig. 4). The specimens were tested to a compressive stress of 350 MPa (0.085% compressive strain); a value that corresponds to approximately 1/10 of their strength in compression. Within this stress range no indication of degradation of the elastic modulus was evident (Fig. 5a). To avoid grain orientation effects (see Sect. 6) a low-magnification objective lens was used. The fluorescence microscope was focused on the central part of the specimen and the loading process was interrupted systematically to allow for collection of the fluorescence spectra (Fig. 5b). The load interruption process did not produce strain relaxation of the material; strain remained constant throughout the duration of the load hold process. To establish the stress-free position of the R line, five spectra had been collected prior to the application of load. The spectra were analyzed in terms of wave-number shifts of the R line from the stress-free value and correlated to the stress value

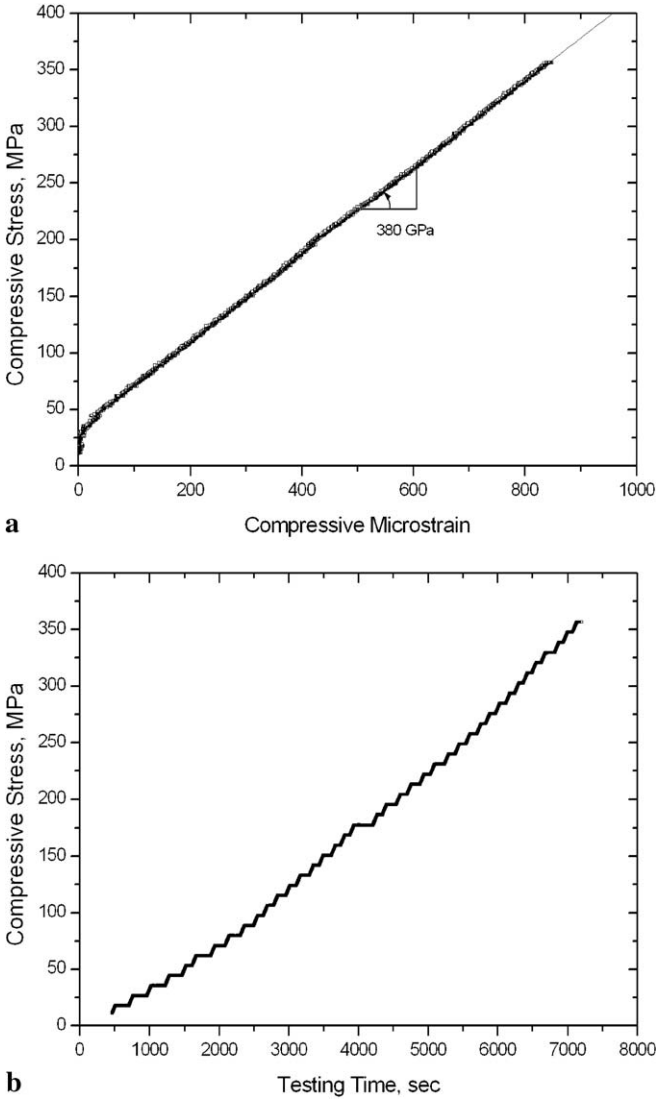

FIGURE 5 Testing of the alumina matrix in axial compression: **a** stress-strain curve; and **b** stress versus testing time curve, showing the load-hold steps associated with the fluorescence measurements

FIGURE 4 Alumina matrix tested in axial compression with simultaneous fluorescence measurements

corresponding to the specific collection instance to obtain the piezo-spectroscopic calibration curve for the alumina matrix (see Sect. 4).

3.3 *Sensitivity of OFM measurements*

3.3.1 Wave-number distributions of the system (shifts inherent to the experimental set-up). To estimate the frequency measurement accuracy inherent to the experimental set-up (standard system error), 100 consecutive R fluorescence spectra were collected on the same position of a Nextel 720 fiber using a laser spot size of one third of the fiber diameter. The R1 and R2 peaks were normally distributed around the reference value with a standard deviation of 0.0593 and 0.0602 cm^{-1}, indicating an error level of ± 0.06 wave-numbers associated with all the spectroscopic measurements.

3.3.2 Wave-number distributions of the sensor in the stress-free state (shifts inherent to the material). To estimate the

self-shift in frequency inherent to the investigated materials two sets of 100 spectra were collected from random sites on the alumina matrix and fibers using a small probe volume. The R1 and R2 lines collected for arbitrary positions and fibers of an as-received Nextel 720 tow were normally distributed around the stress-free value with a standard deviation of 0.049 and 0.036 cm^{-1}, respectively. The corresponding standard deviations of spectra collected using a large laser probe from arbitrary positions on the matrix were 0.064 and 0.062 cm^{-1}, indicative of the higher grain disorientation level of the coarse matrix. Although these measurements already carried the 0.06 cm^{-1} system error, as discussed above, the combined system and sensor errors appear to be of the same value as the system error.

3.3.3 Effect of exposure time/sample heating. Prolonged exposure times of materials under monochromatic radiation, especially at high laser powers, can lead to frequency shifts due to localized thermal energy accumulation in the sensor (heating-up). To estimate the effect of exposure time upon the position of the R line, fixed points on a stress-free alpha-alumina matrix were exposed to the 1 mW laser light radiation and spectra were collected every 3, 30 and 60 s with an integration time of 1 s over a total exposure time of 15 min for each point. The resulting peak frequency distribution was identical to the sensor distribution, a fact that manifested the negligible effect of prolonged exposure on sample heating under the laser power used in this study.

4 Piezo-spectroscopic calibration curves

4.1 *Fibers in tension and compression*

In accordance with the independent measurements, the values of the R1 and R2 lines for the stress-free fibers were found at 14 403 cm^{-1} and 14 433 cm^{-1}, respectively, indicating that no inherent or chemical shifts were present. The piezo-spectroscopic calibration curve for the alumina Nextel 720 fibers is shown in Fig. 6: the position (frequency) of the R1 and R2 lines is plotted against the applied strain and has a symmetric behavior for compressive and tensile loads. The data points exhibit minimal scatter. Figure 6 demonstrates that fiber failure occurred at a strain level of 0.88% in compression and 0.82% in tension, indicating slightly higher fiber endurance in compressive loads as compared to tensile.

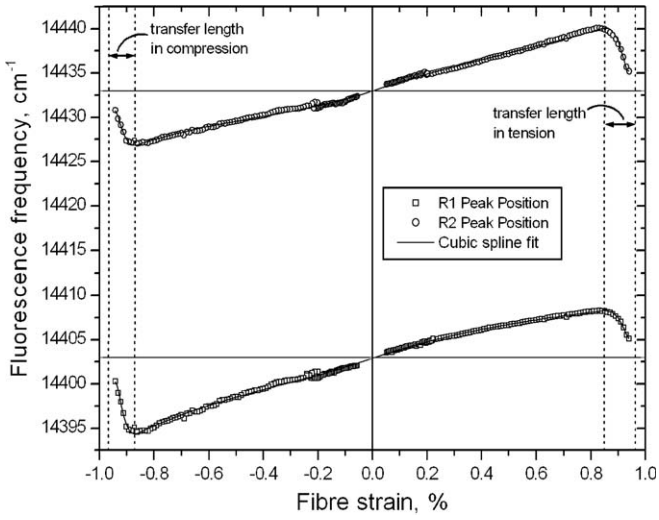

FIGURE 6 Calibration of piezo-spectroscopic effect for the Nextel 720 fibers in tension and compression. *Hollow squares* and *circles* represent the position of the R1 and R2 lines, respectively, whereas *straight lines* are cubic spline fits to the raw data

An unconstrained linear fit within the -0.88% to $+0.82\%$ strain range of Fig. 6 provides an average frequency shift of 7.99 cm^{-1} per strain (%) for the R1 line and 7.57 cm^{-1} per strain for the R2 line. Using the elastic modulus of the fibers, 260 GPa [26, 27], the strain-based values of the piezo-spectroscopic coefficients can be converted to stress-based values; the corresponding coefficients for the R1 and R2 lines

Coefficients a_i of the i^{th}-order term of polynomial regression:
$ff = a_0 + a_1\,\varepsilon + a_2\,\varepsilon^2 + a_3\,\varepsilon^3$
where $ff(\varepsilon)$ =fluorescence frequency [cm^{-1}], ε = strain [%]

Regression type	Line	a_0 (std. error)	a_1 (std. error)	a_2 (std. error)	a_3 (std. error)	Correlation coefficient R^2
Linear	R1	14402.650 [±0.0303]	8.378 [±0.0700]	–	–	0.9931
	R2	14433.275 [±0.0229]	7.812 [±0.0532]	–	–	0.9954
Quadratic	R1	14402.990 [±0.0240]	8.265 [±0.0402]	–1.822 [± 0.0894]	–	0.9956
	R2	14433.092 [±0.0259]	7.843 [±0.0434]	0.988 [± 0.0978]	–	0.9940
Cubic	R1	14403.001 [±0.0226]	8.681 [± 0.0865]	–1.918 [± 0.0856]	–1.084 [± 0.2031]	0.9961
	R2	14433.097 [±0.0250]	8.19 [± 0.0969]	0.948 [± 0.0948]	–0.912 [± 0.2299]	0.9944
			Sum of Squares of Cubic Spline Fit Residuals			
Cubic Spline Fit	R1		5.0			
	R2		6.4			

TABLE 3 Regression parameters for strain-based fiber calibration curves

are 3.07 cm^{-1} GPa^{-1} and 2.91 cm^{-1} GPa^{-1}, respectively. The exact form of the calibration curves was approached through polynomial regressions up to the third order (Table 3). The R1 fluorescence line was found to deviate from linearity, with its quadratic and cubic coefficients being in ratios of 0.22 and 0.12 with the linear-term coefficient. The R2 fluorescence line had an almost linear response to strain, with quadratic and cubic coefficients being fractions 0.12 and 0.11 of their linear counterparts. Additionally, the zero-order-term coefficients (a_0) for the linear regression did not efficiently reproduce the R line position for the stress-free case. In their studies, Melanitis et al. [25] and Filiou and Galiotis [28] noted similar non-linearity effects in the calibration curves of carbon fibers.

He and Clarke [9] have calculated the sum of piezo-spectroscopic coefficients over the three principal crystal directions of chromium-doped sapphire (α-Al_2O_3 single crystal) as: 7.59 cm^{-1} GPa^{-1} and 7.61 cm^{-1} GPa^{-1} for the R1 and R2 lines respectively. In a polycrystalline alumina system, like the Nextel 720 fibers, the effect of polarization on the position of the R line is negligible [21] and, once an optical probe much larger than the grain size is used, the frequency shifts can be averaged over the probed volume [10] to give coefficients for polycrystalline alumina that are 1/3 of the sum of the piezo-spectroscopic coefficients in each direction, i.e. 2.530 cm^{-1} GPa^{-1} and 2.536 cm^{-1} GPa^{-1}, respectively.

The presence of frequency hills and valleys at high strain values in Fig. 6 indicate failure sites during tension and compression, respectively, and is a phenomenon frequently encountered on calibration curves [25]. Moreover, the length of the zone required for the relaxation of stresses (transfer length) is directly associated with the stress-transfer capability of the medium. In our case, the measured transfer length of ca. 5.5 mm is a result of the thin acrylic coating used to bond the fibers to the PMMA beam surface. Different failure sites along the fiber length were pictured using a video copy processor attached to the CCTV camera of the fluorescence microscope. In Fig. 7, images of sequential failures along the length of an alumina fiber tested at the cantilever beam rig are presented. Starting from a simple crack far from the fixed end (image a), damage progresses to catastrophic failure (image d) and, ultimately, fiber overlap (image f) very near the fixed end (maximum strain).

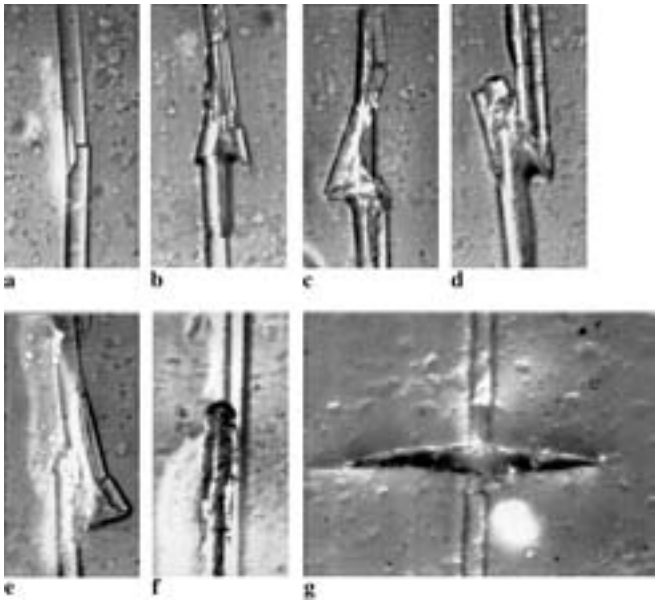

FIGURE 7 The transparent alumina fibers as seen through the fluorescence microscope: images of different failure sites along the fiber during compression (**a**)–(**f**) and tension (**g**) on the cantilever beam rig. A characteristic reference length is the fiber diameter: 12 μm

4.2 *Matrix in compression*

Similar to the fiber case, the values of the R1 and R2 lines for the stress-free matrix were also found at 14 403 cm^{-1} and 14 433 cm^{-1}, respectively. The calibration curve for the matrix is presented in Fig. 8, where the R1 and R2 line positions are plotted against compressive stress. The matrix exhibits some data scattering which appears to be harmonic in magnitude, alternating between negative and positive contributions to the average trend. Noting that the fluorescence measurements were performed in the central part of the specimen, these fluctuations could be attributed to the non-uniform distribution of the applied load within the alumina matrix along the length of the loading axis.

An unconstrained linear fit to the data provides an average frequency shift of 2.57 cm^{-1} GPa^{-1} for the R1 line and 2.52 cm^{-1} GPa^{-1} for the R2 line. The fit parameters are given in Table 4. The offset of the linear regression reproduces effectively the stress-free position of the R1 and R2 lines. As in Fig. 8, the fluorescence frequency can be plotted versus strain-gage-measured strain and fitted to evaluate the strain-based piezo-spectroscopic coefficients. The values of these coefficients for the R1 and R2 line are 9.809 cm^{-1} and 9.618 cm^{-1} per strain percentile, respectively.

The calculated piezo-spectroscopic coefficients for the polycrystalline matrix are equal to the volume average of the sum of the coefficients calculated by He and Clarke [9] for each crystallographic direction.

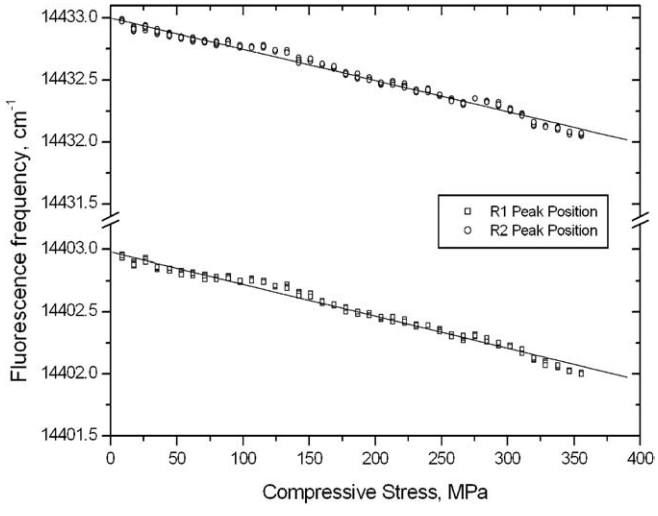

FIGURE 8 Calibration curves for the polycrystalline matrix in compression. *Hollow squares* and *circles* represent the position of the R1 and R2 lines, respectively

Coefficients A and B of linear regression: $ff(\varepsilon) = A + B\,\sigma$ where ff=fluorescence frequency [cm^{-1}], σ = stress [GPa]				
	A [error]	B [error]	Correlation Factor R^2	Standard Deviation
R1 line	14402.979 [±0.00359]	−2.57 [±1.886E − 5]	0.9871	0.0317
R2 line	14432.998 [±0.00355]	−2.52 [±1.864E − 5]	0.9868	0.0313

TABLE 4 Regression parameters for stress-based matrix calibration curves

4.3 *Comparison between matrix and fibers*

The strain-based piezo-spectroscopic coefficients calculated in this study for the polycrystalline alumina fibers have 18% lower values than the corresponding matrix and volume-averaged values. This difference can be explained by the volumetric composition of the Nextel fibers that consist of 85% alpha-alumina and 15% mullite (α-Al_2O_3+3 Al_2O_3·2 SiO_2) in weight concentration terms. Assuming that the fibers are a homogeneous mixture of alpha-alumina and mullite crystallites, the material can be simulated by a system of springs in series where equal stress conditions apply in the two phases during loading. If the densities of the two phases are assumed identical, the ratio of weight concentrations of the two phases equals their relative volume fraction and, hence, the strain taken up by the alpha-alumina crystallites alone (the "effective" alpha-alumina strain) will be 15% lower than the total strain of the two-phase system. Consequently, the strain-based piezo-spectroscopic coefficient of the fibers will be 15% lower than the corresponding effective alpha-alumina coefficient. In fact, the density of alumina is slightly higher than that of mullite and the effective alpha-alumina strain is ca. 17% lower than the total strain of the two-phase system, a finding that is in accordance with the 18% decrease in the piezo-spectroscopic coefficients of the fibers as compared to the corresponding matrix and volume-averaged values.

5 The penetration depth of Al_2O_3

Fluorescence microscopy, as an optical technique, is limited to investigating only those regions of materials that are reachable by the excitation/collection probe. While the outer surfaces of materials can be directly reached by the laser probe, the ability of the technique to collect spectra within the volume of a material depends on the level of transparency of the specific material; a factor that controls the depth at which the incident radiation can penetrate inside the volume of the medium. For example, a black body allows no light penetration by attenuating the incident radiation at the surface, and only its outer surface can be investigated using optical techniques. On the other hand, aluminas are semi-transparent bodies and, as such, allow light to attenuate smoothly within their volume. Laser energy transmission through a transparent medium is governed by Lambert's law: $I(x) = I_0\,e^{-\alpha x}$, where $I(x)$ is the energy of the laser radiation at a depth x below the surface, I_0 is energy at the surface of the medium and α is the absorption coefficient. This phenomenon is generally known as the skin effect and is commonly quantified by the penetration depth, defined as the characteristic distance between the surface of the exposed medium and the depth at which laser energy decreases to 1/e of its incident value. In arithmetical terms, the penetration depth is equal to the inverse absorption coefficient. The penetration depth is a material property dependent on the electromagnetic properties of the medium (electric resistivity, magnetic permeability) but it is also a function of external parameters such as the wavelength of the incident radiation, temperature, angle of incidence and plane of polarization.

As much as a large penetration depth is desirable in fluorescence and Raman spectroscopy, as it expands the resolution of these techniques, attention has to be paid when probing transparent bodies with internal stress gradients below the probed surface, in that the collected spectra will essentially capture the whole stress gradient. This phenomenon is of particular importance when the focal depth (the distance over which the beam diameter remains practically unchanged) of the collecting lens is large enough to retain focus within a large depth inside the medium. In other words, the presence of stress gradients within the probed volume of a material of large penetration depth in conjunction with the use of an optical system of large focal depth results in the collection of spectra that are convoluted in frequencies corresponding to every stress level encountered within the probed volume. Under such conditions, no apparent relation can be drawn between the frequency shifts and the stress state of the sensor.

For example, the cantilever beam technique described in a previous section is excellent for piezo-spectroscopic measurements of thin deformed fibers as stress is uniform along the fiber cross section. Would the same bending technique be applied for the case of an alumina beam (Fig. 9), the laser probe would penetrate to a significant depth below the surface and would capture the stress gradient along the beam thickness. In that case, the resultant spectra would be broad enough to account for all the different stress levels captured.

The focal depth associated with the specific collecting lens, laser wavelength and beam characteristics is of the order of 0.5 mm; thus, given a material with a large penetration depth, the laser probe could potentially capture information from a considerable depth below the surface. The penetration depth of alumina, δ^*, was measured for the monochromatic radiation of this study (wavelength of 514.5 nm) using the fol-

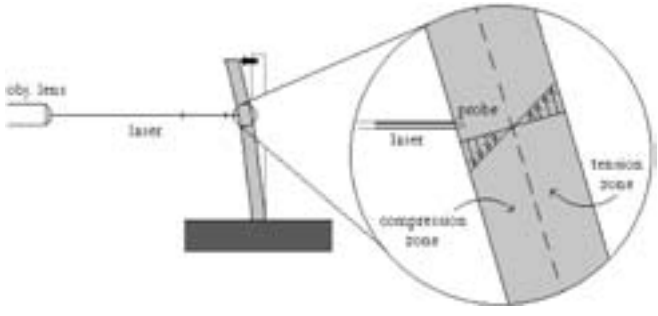

FIGURE 9 Representation of the optical skin problem in an alumina beam with an internal stress gradient due to bending. The laser probe penetrates to a significant depth inside the semi-transparent material and collects information from the different stress levels present in the probed volume

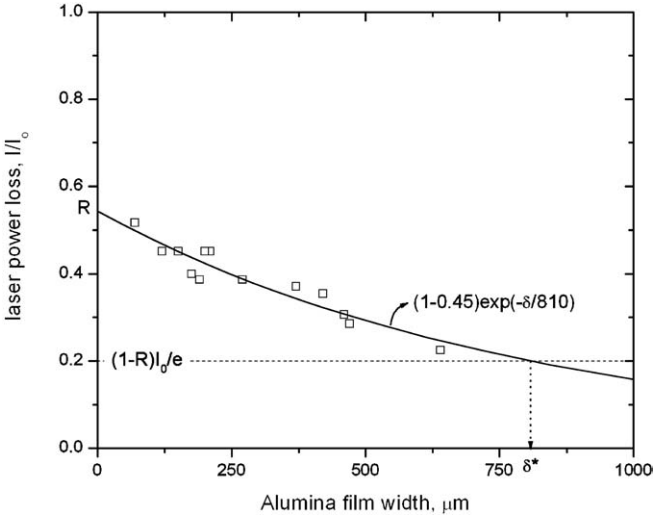

FIGURE 10 The penetration depth of dense alumina at a wavelength of 514.5 nm. *Hollow squares* represent experimental measurements whereas the *solid line* is the optimal regression of the type $(1-R)\exp(-x/\delta^*)$ where R is the reflectivity of alumina and δ^* is the penetration depth

lowing technique: alumina films of various thicknesses were cut from untested matrix specimens using a diamond disk saw (Buehler Isomet 1000 precision saw) and the power loss through the film was measured using a power meter equipped with a light-sensitive sensor. Since the laser power at the surface of the medium could not be measured directly, Lambert's law had to be modified to account for the portion of the incident energy that was reflected at the surface: $I(x) = [(1-R)\,I_0] \times e^{-\frac{x}{\delta^*}}$, where R is the reflectivity of alumina. The power loss versus alumina film thickness is plotted in Fig. 10. The laser power has decreased to $(1-R)\,I_0/e$ or 37% of the laser energy at the surface at a depth of $\delta^* = 810\ \mu m$, the penetration depth.

6 Effect of probe volume

The alumina crystal consists of Al^{3+}, O^{2-} and trace Cr^{3+} ions in an ionic structure that is oriented along three principal mutually-orthogonal crystallographic axes (namely a, c and m) and, as discussed previously, a piezo-spectroscopic coefficient is applicable for each crystallographic direction [5]. Accordingly, the frequency shift, $\Delta\nu$, can be related to stress through the equation:

$$\Delta\nu = \Pi_{ij}\sigma^*_{ij} \tag{2}$$

where Π_{ij} is the tensor of piezo-spectroscopic coefficients and σ^*_{ij} is the stress state defined in the crystallographic basis of the host alumina lattice. In (2), the second- and higher-order terms have been neglected for simplicity. The first- and second-order piezo-spectroscopic coefficients for a α-Al_2O_3 single crystal have been calculated along the three principal crystallographic directions by He and Clarke [9].

Polycrystalline alumina systems, such as the fibers and matrices used in this study, consist of a large number of grains that are randomly oriented with respect to each other. Each grain can be considered as a small crystal with its own local orthogonal coordinate system that is also randomly oriented with respect to that of the neighbouring grains. It seems rational that in order to quantify the frequency shift in such a system using (2), one needs to know all the crystallographic orientations of the excited grains and the corresponding stress state in each direction. However, this limitation can be overcome by using a probe volume that is much larger than the average grain size of the medium investigated and renders the local grain orientation unimportant. Then, the laser probe "sees" the surface as a homogeneous medium by averaging over a large number of grains and hence capturing all possible orientations. Accordingly, the frequency shift of the R line will be the average over all possible piezo-spectroscopic coefficients [13]:

$$\overline{\Delta\nu} = \frac{\Pi_{ij}}{3}\,\sigma_{ij} \tag{3}$$

Depending on the average grain size of the target media used in this study, the volume of the excitation/collection laser probe was controlled by means of objective lenses of different magnification powers. The diameters of the laser spots obtained for each lens were estimated using a micro grid and

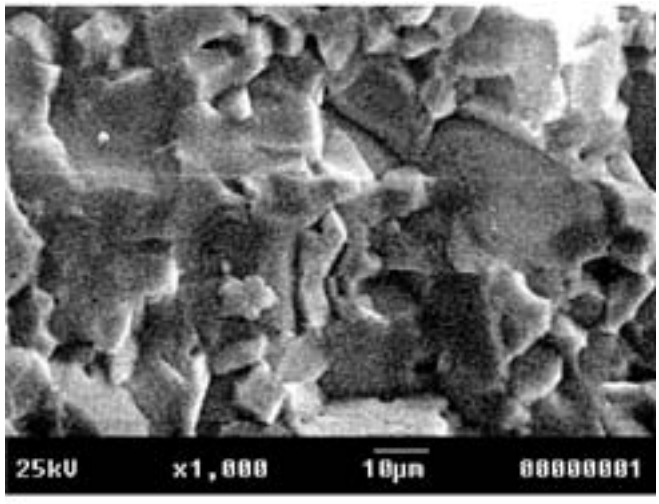

FIGURE 11 SEM images of the matrix (**a**) and fiber (**b**) surfaces used to determine the grain sizes and, subsequently, the probe volume to be implemented

a reference length of 10 μm. Average grain sizes for the matrix and fibers were estimated by means of scanning electron microscopy (Fig. 11). The matrix grains appeared coarse, highly disorganized and randomly oriented with sizes between 5 and 10 μm; this fact dictated the use of a large laser probe that could capture a significant number of random grains. A × 4 objective lens was used for the matrix measurements, which yielded a laser spot of ca. 70 μm in cross-sectional diameter, hence ensuring collection of all possible orientations. The surface morphology of the alumina fibers showed fine grains of characteristic dimensions of less than 0.10 μm (Fig. 11a). Accordingly, for the fiber OFM measurements, an objective lens with a ×50 magnifying power was chosen to yield a laser spot of 4 μm in diameter, approximately 1/3 of the fiber diameter, thus allowing for high spatial resolutions without the probe being able to distinguish any morphology on the fiber surface.

To demonstrate the effect of the dimensions of the probe volume upon the position of the R line for the stress-free material, 100 spectra were collected from equal-in-number random sites on the alumina matrix using two different objective lenses: ×50 and ×10 in magnification power (laser probe sizes 4 μm and 40 μm, respectively, compared to average matrix grain size of 5–10 μm). The fluorescence frequency of the R1 and R2 lines was plotted as a function of random position (Fig. 12a). Spectra collected with the low-magnification lens (corresponding to a bigger probe volume) were distributed normally around the stress-free value with a standard deviation of 0.02 cm^{-1}. Spectra collected on the matrix using the high-magnification lens (corresponding to a smaller probe volume) were distributed normally around the stress-free value with a standard deviation of 0.06 cm^{-1}, three times bigger than the previous value. Additionally, the intensity ratio of the R1 and R2 fluorescence lines, a measure of the optical axis of an α-Al_2O_3 crystal [21], is plotted as a function of arbitrary position (Fig. 12b). Figure 12a and b demonstrates that a probe volume with dimensions comparable to the average grain size of the sensor results in frequency shifts from the stress-free reference position as a result of the preferential orientation of the captured grain. As an additional remark, it has to be stated that the spectroscopic set-up used in this study was equipped with polarization-preserving fiber optics for delivery and collection of laser light with the polarization axis being parallel to the loading axis (for matrix tests) or the fiber length. However it has been proven [21] that the effect of polarization on (2) for the case of Cr^{3+} fluorescence from polycrystalline alumina is negligible.

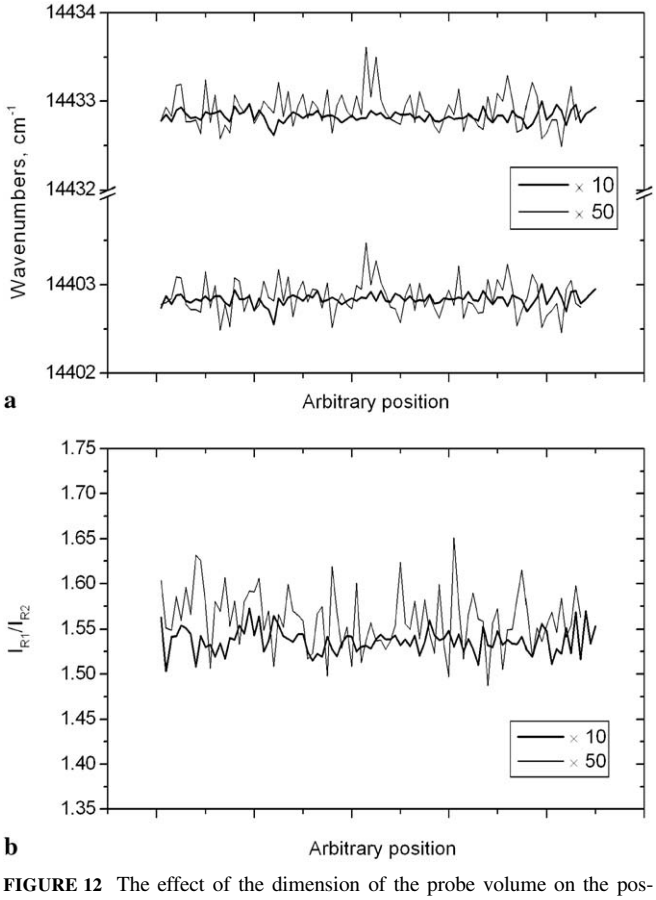

FIGURE 12 The effect of the dimension of the probe volume on the position of the R-fluorescence line for the stress-free alumina matrix. *Thin* and *thick lines* represent results with probe volumes that are comparable to – and much larger than – the average grain size, respectively. **a** The absolute position of the R1 and R2 fluorescence lines. **b** The R1-to-R2 line intensity ratio, a mirror of the optical axis of an α-Al_2O_3 grain

7 Applications

7.1 *Residual stresses in Nextel 720 fibers due to sizing*

The as-received Nextel 720 alumina fibers were coated with a PVA (polyvinyl alcohol)-based sizing for ease of handling. In a simplified approach, the sized fibers can be considered as a composite cylinder system with the fiber being the internal core, embedded in a coaxial cylindrical shell, the outer sizing. Residual stresses can develop in the constituents during temperature changes due to the thermal expansion mismatch between the fiber and the coating. To explore the presence of residual stresses on the Nextel 720

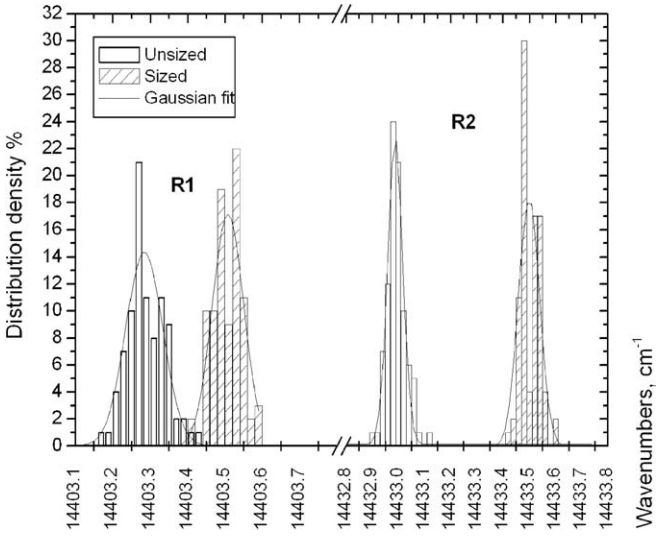

FIGURE 13 The R fluorescence peak distributions for the sized and unsized fibers. *Hollow* and *striped columns* stand for the sized and unsized fibers, respectively, whereas *straight lines* represent the Gaussian approximations to the raw data

fibers due to the presence of the sizing, 100 spectra were collected at random positions on as-received (sized) and desized fibers in tows, and the positions of the R1 and R2 lines were compared. The desizing procedure involved heat cleaning of the tow in 700 °C for 5 min. This was achieved in a ventilated furnace where heat was applied at a rate of 300 °C/h. As a result of the sizing removal, fibers lost 2% of their initial mass and appeared white, as compared to the sized fibers, which had an off-white color. Sized and unsized fibers were scanned with the fluorescence microscope and the spectra were analyzed in terms of the R line position. The results are presented in Fig. 13. The R1 and R2 lines of the sized fibers appear higher by 0.2 and 0.5 wavenumbers (cm^{-1}), respectively, than those for the unsized fibers. Using the piezo-spectroscopic calibration curve for the fibers presented earlier, these shifts indicate that the presence of sizing imposes residual tensile strains of the order of 0.05%.

7.2 *Strain mapping of residual stresses in thermally grown oxides*

The OFM technique was applied to evaluate the residual stresses developed in the thermally grown oxide (TGO) phase of a thermal barrier-coating coupon that had already failed after testing in thermomechanical fatigue (TMF). The system consisted of a central superalloy core of cylindrical cross section covered radially by a bond coat and a thermal barrier coating (Fig. 14). The superalloy consisted partially of aluminum, which under the high temperatures of TMF testing had oxidized to form aluminum oxide.

Fluorescence spectra were collected using a ×10 objective lens, which produced a large probe volume with a laser spot diameter of ca. 40 μm. The reference R line position was determined at a collection point outside the gauge length of the specimen by rotating the sample to a vertical position in order to focus on the thermally grown alumina (Fig. 16a). The reference R fluorescence line of the sample appeared at higher frequencies with respect to the stress-free value obtained from the alumina matrix experiments. Specifically, the positions of the reference R1 and R2 lines were higher by 1.5 and 2.5 wave-numbers (cm^{-1}), respectively, than the matrix values (Fig. 15). This shift is considered to be chemical in nature and can be attributed to the thermal treatment that the oxide received during residence at high temperatures during TMF testing.

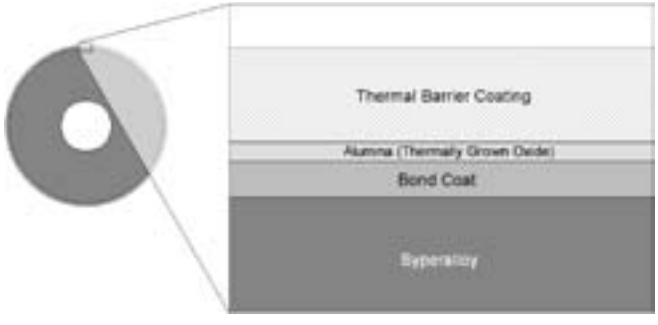

FIGURE 14 Schematic representation of the cross section of the coupon showing the bond-coated superalloy, the thermal barrier coating and the location of the TGO (graphic is not to scale)

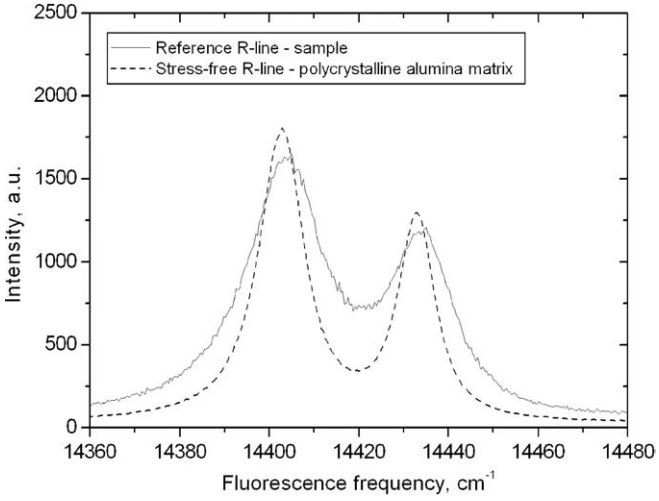

FIGURE 15 The reference R line of the thermally grown alumina plotted together with the R line of the stress-free alumina matrix. Shifting and line broadening effects inherent to the thermally grown alumina are characteristic of the existence of internal stresses

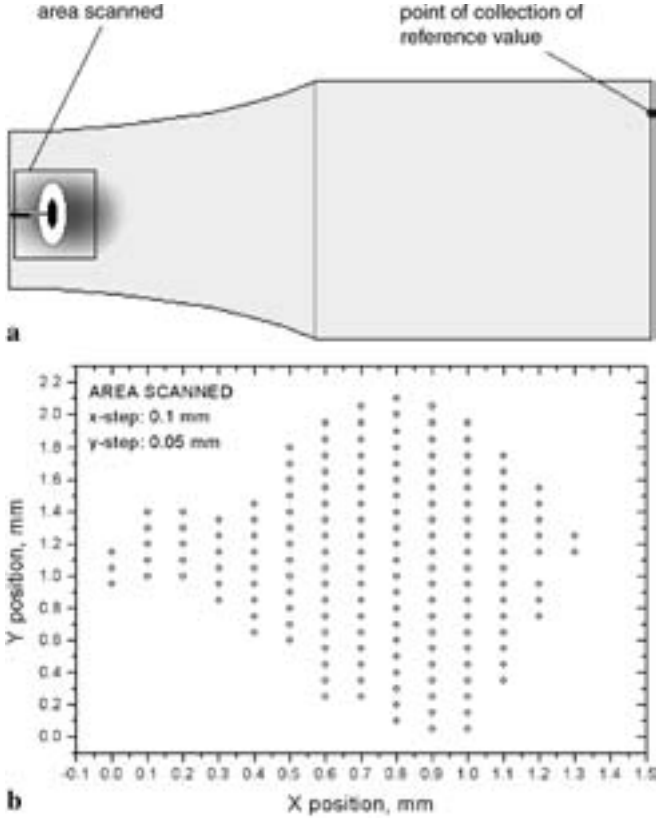

FIGURE 16 TBC coupon: **a** the scanned area and the point of collection of the reference R line position and **b** map of collection points

Probing the thermally grown oxide at any given region of the sample was impossible, as the thermal barrier coating was almost impenetrable to laser light. Using the fluorescence probe, a 3-mm^2 damage area near the neck of the failed specimen was investigated where the thermal barrier coating had spalled, revealing the thermally grown oxide. The area was scanned with a step of 0.05 mm along the principal axis

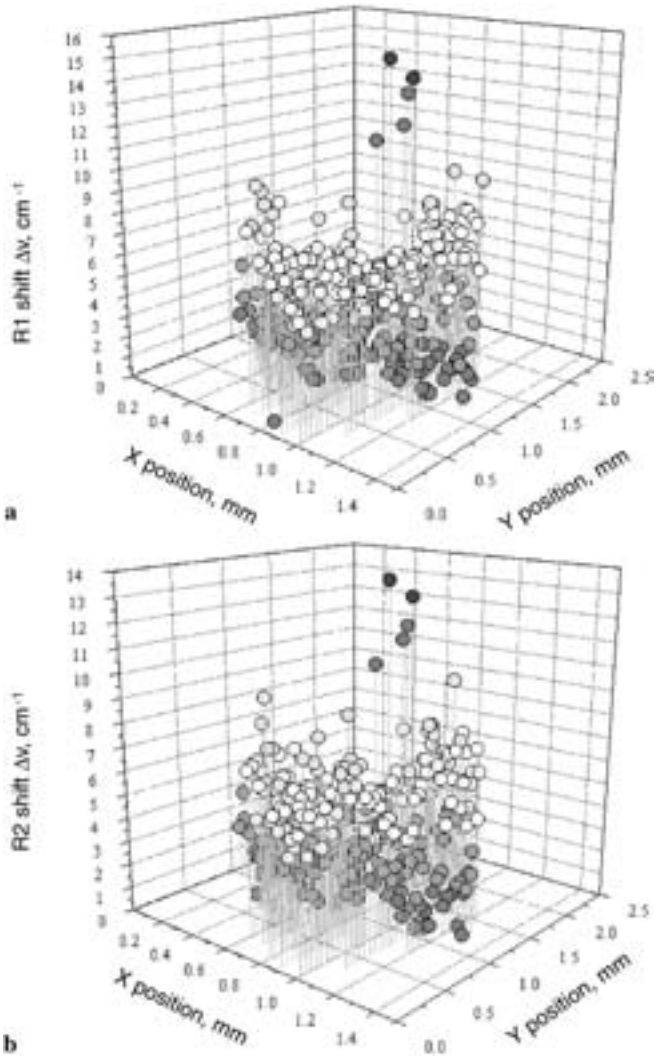

FIGURE 17 Strain mapping of the damage area: frequency shifts of the R1 (**a**) and R2 (**b**) lines from the reference value

of the specimen and a step of 0.1 mm in the circumferential direction (Fig. 16).

The results of fluorescence frequency shifts from the reference value are plotted in absolute values as a function of the collection position in Fig. 17a and b. Using the piezo-spectroscopic coefficients obtained for the R2 line for the alumina matrix, the observed shifts of the R2 line can be related to residual stress. Neglecting the contributions of four extreme points at shifts greater than $10\,\mathrm{cm}^{-1}$, the mean shift of the R2 line was calculated as $3.23\,\mathrm{cm}^{-1}$, corresponding to a residual compressive strain of 1.28 GPa.

8 Conclusions

The micromechanics of α-Al_2O_3 constituents were quantified by means of optical fluorescence microscopy. Polycrystalline fibers and matrix specimens were tested at room temperature and the piezo-spectroscopic effect was calibrated to provide the basis of frequency shift measurements in real composites in terms of stresses and strains. Fine-grained Nextel 720 single-filament specimens were tested in tension and compression using the cantilever beam technique, whereas the matrix specimens where tested only under axial compression. The piezo-spectroscopic behavior was determined in situ and the corresponding coefficients for both constituents were determined. The piezo-spectroscopic coefficients of the polycrystalline matrix were found to be of $2.57\,\mathrm{cm}^{-1}\,\mathrm{GPa}^{-1}$ for the R1 line and $2.52\,\mathrm{cm}^{-1}\,\mathrm{GPa}^{-1}$ for the R2 line, equal to the volume-averaged values obtained for α-Al_2O_3 single crystals in previous studies. The coefficients for the polycrystalline α-Al_2O_3 Nextel 720 fibers where found to be $7.99\,\mathrm{cm}^{-1}$ and $7.57\,\mathrm{cm}^{-1}$ per strain or $3.07\,\mathrm{cm}^{-1}\,\mathrm{GPa}^{-1}$ and $2.91\,\mathrm{cm}^{-1}\,\mathrm{GPa}^{-1}$ for the R1 and R2 lines, respectively. The decrease in the strain-based piezo-spectroscopic coefficients of the fibers, as compared with their single-crystal volume-averaged counterparts, is directly related to the presence of a second phase (mullite) in the composition of the fibers. The effective alpha-alumina piezo-spectroscopic coefficients, calculated under the assumption of equal stress conditions in the alumina and mullite crystallites in the fibers, were equal to the volume-averaged single-crystal values. The effect of the fluorescence probe volume and its significance in the OFM technique was analyzed with respect to the average grain size of the target sensor. The penetration depth of polycrystalline α-Al_2O_3 matrix was calculated experimentally to be of the order of $810\,\mu\mathrm{m}$. The piezo-spectroscopic calibration was inversely applied to estimate a residual stress level of ca. 1.3 GPa in the thermally grown oxide of a thermal barrier coating system, as well as to calculate the effect of sizing on the internal stress state of the fibers.

ACKNOWLEDGEMENTS The authors wish to thank Dr.Ir.M. Steen and Dr.H. Mullejans of the Institute for Advanced Materials, Joint Research Center, European Commission, Petten, The Netherlands for their support throughout this study.

REFERENCES

1 *CRC Materials Science and Engineering Handbook*, 3rd edn. (CRC Press LLC, Boca Raton, Florida 2001)
2 S. Suguno, Y. Tanab: J. Phys. Soc. Jpn. **13**, 880 (1958)
3 S. Suguno, I. Tsujikaw: J. Phys. Soc. Jpn. **13**, 899 (1958)
4 D. McClure: J. Chem. Phys. **36**, 3118 (1962)
5 L. Grabner: J. Appl. Phys. **49**, 580 (1978)
6 R.A. Forman, G.J. Piermarini, J.D. Barnett, S. Block: Science **176**, 284 (1972)
7 G.J. Piermarini, S. Block, J.D. Barnett, R.A. Forman: J. Appl. Phys. **46**, 2774 (1975)
8 Q. Ma, D.R. Clarke: Acta Metall. Mater. **41**, 1811 (1993)
9 J. He, D.R. Clarke: J. Am. Ceram. Soc. **78**, 1347 (1995)
10 Q. Ma, D.R. Clarke: J. Am. Ceram. Soc. **76**, 1433 (1993)
11 Q. Ma, D.R. Clarke: Acta Metall. Mater. **41**, 1817 (1993)
12 R.J. Young, X. Yang: Composites A **27**, 737 (1996)
13 J. He, D.R. Clarke: Proc. R. Soc. Lon. A **453**, 1881 (1997)
14 D.M. Lipkin, D.R. Clarke: Oxidation of Metals **45**, 267 (1996)
15 R. Christensen, D.M. Lipkin, D.R. Clarke, K. Murphy: Appl. Phys. Lett. **69**, 3754 (1996)
16 D.M. Lipkin, D.R. Clarke, M. Hollatz, M. Bobeth, W. Pompe: Corrosion Sci. **39**, 231 (1997)
17 V.K. Tolpygo, J. Dryden, D.R. Clarke: Acta Mater. **46**, 927 (1998)
18 G. Pezzotti, H. Okuda, N. Muraki, T. Nishida: J. European Ceramic Soc. **19**, 601 (1999)
19 G. Pezzotti, H. Suenobu, T. Nishida: J.Am. Ceramic Soc. **82**, 1257 (1999)
20 G. Pezzotti, O. Sbaizero, V. Sergo, N. Muraki, K. Maruyama, T. Nishida: J.Am. Ceramic Soc. **81**, 187 (1998)
21 J. He, D.R. Clarke: J. Am. Ceram. Soc. **80**, 69 (1997)

22 A. Paipetis, C. Vlattas, C. Galiotis: J. Raman Spect. **27**, 519 (1996)
23 L.S. Schadler, C. Galiotis: Int. Mat. Rev. **40**, 116 (1995)
24 C. Galiotis: *Micromechanics of Reinforcement using Laser Raman Spectroscopy, Microstructural Characterisation of Fiber-Reinforced Composites* (Woodhead Publishing Ltd., Cambridge, England 1998) pp. 224–253
25 N. Melanitis: *Ph.D. Thesis* (Queen Mary and Westfield College, Department of Materials, University of London 1991)
26 3M Corporation: *3M Nextel Ceramic Fiber Technical Notebook* (http://www.3m.com/ceramics, 1999)
27 K.G. Dassios, M. Steen, C. Filiou: Mater. Sci. Eng. A (2003), in press
28 C. Filiou, C. Galiotis: Composites Sci. Tech. **59**, 2149 (1999)